

# POLARIZED SCATTERING WITH PASCHEN-BACK EFFECT, HYPERFINE STRUCTURE, AND PARTIAL FREQUENCY REDISTRIBUTION IN MAGNETIZED STELLAR ATMOSPHERES

K. SOWMYA<sup>1</sup>, K. N. NAGENDRA<sup>1</sup>, J. O. STENFLO<sup>2,3</sup> AND M. SAMPOORNA<sup>1</sup>

<sup>1</sup>*Indian Institute of Astrophysics, Koramangala, Bengaluru, India*

<sup>2</sup>*Institute of Astronomy, ETH Zurich, CH-8093 Zurich, Switzerland*

<sup>3</sup>*Istituto Ricerche Solari Locarno, Via Patocchi, 6605 Locarno-Monti, Switzerland*

ksowmya@iiap.res.in; knn@iiap.res.in; stenflo@astro.phys.ethz.ch; sampoorna@iiap.res.in

## ABSTRACT

$F$ -state interference significantly modifies the polarization produced by scattering processes in the solar atmosphere. Its signature in the emergent Stokes spectrum in the absence of magnetic fields is depolarization in the line core. In the present paper, we derive the partial frequency redistribution (PRD) matrix that includes interference between the upper hyperfine structure states of a two-level atom in the presence of magnetic fields of arbitrary strengths. The theory is applied to the Na I D<sub>2</sub> line that is produced by the transition between the lower  $J = 1/2$  and upper  $J = 3/2$  states which split into  $F$  states because of the coupling with the nuclear spin  $I_s = 3/2$ . The properties of the PRD matrix for the single-scattering case is explored, in particular, the effects of the magnetic field in the Paschen–Back regime and their usefulness as a tool for the diagnostics of solar magnetic fields.

*Subject headings:* atomic processes – line: formation – magnetic fields – polarization – scattering – Sun: atmosphere

## 1. INTRODUCTION

The atomic energy levels are split into magnetic substates in the presence of a magnetic field. When the magnetic splitting is much smaller than the separation between the hyperfine structure states, then we are in the Zeeman regime. In this regime, the energy shift produced by the magnetic field varies linearly with the field strength. On the other hand, if the magnetic splitting is comparable to or larger than the energy difference between the hyperfine structure states, then the magnetic field effects are described by the Paschen–Back effect (PBE) in which the magnetic splitting varies nonlinearly with the magnetic field strength, leading to level-crossing interference effects. The Hanle effect represents a modification of the resonance scattering polarization by the mag-

netic field. In the present paper, we are concerned with the Hanle effect involving hyperfine structure states. This leads to several interesting phenomena related to level-crossing interferences.

Hyperfine structure splitting (HFS) is generally much smaller when compared to fine structure splitting. Therefore, for those field strengths for which we are still in the Zeeman regime in the case of fine structure states, we may already be in the regime where PBE is operating on hyperfine structure states. PBE becomes important in studies of lines showing hyperfine structure when they are formed in the magnetic regions on the Sun.

PBE in molecular lines have been extensively studied both in the context of solar and stellar physics. Molecular PBE gives signatures in the Stokes profiles, which serve as a promising tool for diagnosis of solar and stellar magnetic

fields (see, e.g., Berdyugina et al. 2005, 2006a,b; Shapiro et al. 2006, 2007; Asensio Ramos 2006). As in the case of molecular lines, PBE also occurs in atomic lines. The influence of PBE on emergent profiles of atomic lines such as the He I 10830 Å multiplet, Fe II multiplet, Si II, Si III etc., have been studied (see, e.g., Bommier 1980; Sasso et al. 2006; Stift et al. 2008; Stift & Leone 2008; Khalack & Landstreet 2012).

Landi Degl’Innocenti (1975) formulated the transfer equation for a line with hyperfine structure in the presence of a magnetic field, both in LTE and NLTE. He also presented expressions for strengths and shifts of the magnetic components of the lines formed due to transitions between hyperfine structure states. A Fortran program to compute these strengths and magnetic shifts was made available in a later paper by the same author (see Landi Degl’Innocenti 1978). We use this computer program to calculate the eigenvalues and expansion coefficients discussed in Section 3. Lopez Ariste et al. (2002) discussed the net circular polarization induced by the hyperfine structure and its usefulness as a tool for the diagnosis of solar magnetic fields in the quiet photosphere and plages.

The interference between hyperfine structure states (called the  $F$ -state interference phenomenon) plays a significant role in modifying the shapes of the emergent Stokes profiles. Stenflo (1997) developed a scattering theory of quantum interference phenomena which explains the effect of  $F$ -state interference on coherently scattered lines. Landi Degl’Innocenti & Landolfi (2004, hereafter LL04) have developed a QED theory to handle  $F$ -state interference phenomenon in the PB regime for scattering on a multi-level atom under the approximation of complete frequency redistribution (CRD). Casini & Manso Sainz (2005) discuss the same problem but for scattering on a multi-term atom that includes both  $J$ -state and  $F$ -state interference phenomena again under the approximation of CRD. Using the theory of LL04, Belluzzi et al. (2007) and Belluzzi (2009) investigated the effects of magnetic field on lines resulting from transitions between hyperfine structure states of odd isotope of Ba and Sc II, respectively.

A scattering theory of  $F$ -state interference based on a metalevel approach was developed by Landi Degl’Innocenti et al. (1997). This theory

takes into account PRD in the collisionless regime. In Smitha et al. (2012), we presented the PRD matrix for the  $F$ -state interference phenomenon in the absence of magnetic fields and in the collisionless regime. This PRD theory was applied in Smitha et al. (2013) to illustrate the importance of PRD, HFS, isotopic shifts, and radiative transfer in modeling the observed non-magnetic linear polarization profiles of Ba II D<sub>2</sub> 4554 Å line. In the present paper, we derive the PRD matrix for a two-level atom with HFS in the presence of a magnetic field of arbitrary strength. A straightforward extension of the  $J$ -state redistribution matrix (RM) presented in Smitha et al. (2011) to the case of  $F$ -state interference in the PB regime is not possible because the RM derived in that paper is valid only in the linear Zeeman regime. Therefore, in the present paper, we formulate the theory of  $F$ -state interference in the PB regime and derive an expression for the RM including PRD in the absence of collisions. We assume the lower levels to be infinitely sharp and unpolarized. For the sake of clarity, in Section 2 we describe the atomic system on which the magnetic field acts. The atom-radiation interaction in the presence of a magnetic field of arbitrary strength is discussed quantitatively in Section 3. In Section 4 we present the characteristics of the RM derived in Section 3. Concluding remarks are presented in Section 5.

## 2. THE ATOMIC SYSTEM

The atomic system that we consider has two  $J$ -states (where  $J$  is the total electronic angular momentum) belonging to two different terms. The lower state is labeled  $J_a$  ( $= J_f$ , the final state), and the upper state  $J_b$ . When the atomic nucleus possesses a spin  $I_s$ , the coupling between  $J$  and  $I_s$  results in hyperfine structure states  $F$  so that  $\mathbf{F} = \mathbf{J} + \mathbf{I}_s$ . The  $F$  states are given by the vector addition formula  $F = |J - I_s|, \dots, J + I_s$ . The number of  $F$  states into which a given  $J$  state splits is given by  $\min(2J + 1, 2I_s + 1)$ . For electric dipole transitions between the  $F$  states the selection rules are  $\Delta J = 0, \pm 1$ ,  $\Delta F = 0, \pm 1$ , and  $\Delta \mu = 0, \pm 1$  in the Zeeman regime and  $\Delta J = 0, \pm 1$  and  $\Delta \mu = 0, \pm 1$  in the PB regime. Here,  $\mu$  denotes the magnetic substates of the hyperfine structure states. The electric dipole nature of the interaction does not permit transitions among  $F$  states

of a given  $J$  state.

The hyperfine structure of an element has dominant contributions from magnetic dipole and electric quadrupole interactions (see Corney 1977; Woodgate 1992). The Hamiltonian  $\mathcal{H}_D$  describing the interaction of the nuclear magnetic moment with the magnetic field produced at the nucleus by the valence electrons can be written as

$$\mathcal{H}_D = \mathcal{A}_J \mathbf{I}_s \cdot \mathbf{J} , \quad (1)$$

where  $\mathcal{A}_J$  is the magnetic dipole hyperfine structure constant and is mostly determined from experiments. The Hamiltonian  $\mathcal{H}_Q$  for the electric quadrupole interaction between the protons and electrons due to the finite extent of the nuclear charge distribution is given by

$$\mathcal{H}_Q = \frac{\mathcal{B}_J}{2I_s(2I_s - 1)J(2J - 1)} \times \left\{ 3(\mathbf{I}_s \cdot \mathbf{J})^2 + \frac{3}{2}(\mathbf{I}_s \cdot \mathbf{J}) - I_s(I_s + 1)J(J + 1) \right\} \quad (2)$$

where  $\mathcal{B}_J$  is the electric quadrupole hyperfine structure constant which is also in most cases determined by experimental measurements.

The total Hamiltonian for the atomic system in the presence of an external magnetic field is written as

$$\mathcal{H} = \mathcal{H}_0 + \mathcal{H}_{\text{hfs}} + \mathcal{H}_B , \quad (3)$$

where  $\mathcal{H}_0$  is the Hamiltonian describing the atomic structure excluding hyperfine structure and  $\mathcal{H}_{\text{hfs}}$  is the Hamiltonian for the hyperfine structure interaction which, is the sum of  $\mathcal{H}_D$  and  $\mathcal{H}_Q$ .

In the absence of an external magnetic field, the hyperfine interaction energy  $E_{\text{hfs}}$  is given by

$$E_{\text{hfs}} = \frac{1}{2} \mathcal{A}_J \mathcal{K} + \frac{\mathcal{B}_J}{8I_s(2I_s - 1)J(2J - 1)} \times \{ 3\mathcal{K}(\mathcal{K} + 1) - 4J(J + 1)I_s(I_s + 1) \} , \quad (4)$$

where  $\mathcal{K} = F(F + 1) - J(J + 1) - I_s(I_s + 1)$ .

In the limit of  $\mathcal{B}_J \ll \mathcal{A}_J$ , the spacing between the  $F$  states is given by the so-called hyperfine structure interval rule

$$\Delta E = E_F - E_{F-1} = \mathcal{A}_J F . \quad (5)$$

In cases where  $\mathcal{B}_J$  is finite, an additional energy shift is produced.

The magnetic Hamiltonian  $\mathcal{H}_B$  in Equation (3) has the form

$$\mathcal{H}_B = \mu_0 (\mathbf{L} + 2\mathbf{S}) \cdot \mathbf{B} = \mu_0 B (J_z + S_z) , \quad (6)$$

where  $\mu_0$  is the Bohr magneton. The  $z$  axis of the coordinate system is assumed to be along the magnetic field direction. In the PB regime, the magnetic field produces a splitting comparable with the separation between the  $F$  states. In such cases, the magnetic substates of a given  $F$  state can superpose on the magnetic substates of another  $F$  state. This leads to a mixing of  $F$  states. Such a mixing of states can occur even for very small values of field strengths. The purpose of this paper is to derive an expression for the PRD matrix representing the  $F$ -state interference process in the PB regime.

### 3. REDISTRIBUTION MATRIX

In the scattering theory approach, the physics of atom radiation interaction is described through the so-called RM in the astrophysical literature. It describes the correlations between the incident and scattered photon frequencies, angles, and polarizations.

#### 3.1. PB Regime

The PB regime is reached when the Zeeman splitting of the magnetic substates  $\mu$  belonging to a given  $F$  state becomes comparable to the energy separations between the  $F$  states themselves. This is generally referred to as the incomplete PB effect. In such a situation, the magnetic field can no longer be treated as a perturbation to the atom-radiation interaction, and one has to carry out a simultaneous diagonalization of the hyperfine interaction and magnetic Hamiltonians.

The Kramers–Heisenberg formula, which gives the complex probability amplitudes for scattering from an initial magnetic substate  $a$  to a final substate  $f$  through intermediate states  $b$ , is written as

$$w_{\alpha\beta} \sim \sum_b \frac{\langle f | \mathbf{r} \cdot \mathbf{e}_\alpha | b \rangle \langle b | \mathbf{r} \cdot \mathbf{e}_\beta | a \rangle}{\omega_{bf} - \omega - i\gamma/2} . \quad (7)$$

Here,  $\omega = 2\pi\xi$  is the circular frequency of the scattered radiation.  $\hbar\omega_{bf}$  is the energy difference between the excited and final levels, and  $\gamma$  is the damping constant.

The coherency matrix for this scattering process  $a \rightarrow b \rightarrow f$  is given by

$$\mathbf{W} = \sum_a \sum_f \mathbf{w} \otimes \mathbf{w}^* . \quad (8)$$

The incoherent summation is taken over the initial and final levels (see Stenflo 1998). Here,  $\mathbf{w}$  is the Jones matrix, and its elements are given by Equation (7).

We first identify the basis vectors  $|a\rangle$ ,  $|b\rangle$ , and  $|f\rangle$  in the PB regime as

$$|a\rangle = |J_a I_s i_a \mu_a\rangle , \quad (9)$$

with similar forms for  $|b\rangle$  and  $|f\rangle$ . We then expand these PB regime basis vectors in terms of basis vectors  $|J I_s F \mu\rangle$  of the Zeeman regime as

$$|J_a I_s i_a \mu_a\rangle = \sum_{F_a} C_{F_a}^{i_a}(J_a I_s, \mu_a) |J_a I_s F_a \mu_a\rangle , \quad (10)$$

with similar expansions carried out for intermediate and final state vectors. The  $C$  coefficients appearing in the above equation are given by

$$C_F^i(J I_s, \mu) = \langle J I_s F \mu | J I_s i \mu \rangle , \quad (11)$$

which can be assumed to be real because the total Hamiltonian is real.

Using Equation (10) in the Kramers–Heisenberg formula and noting that  $J_f = J_a$ , the dipole matrix elements can be expanded using the Wigner–Eckart theorem (see Equations. (2.96) and (2.108) of LL04) to obtain

$$\begin{aligned} w_{\alpha\beta} &\sim \sum_{i_b \mu_b} \sum_{F_a F_f F_b F_{b''}} \sum_{q q''} (-1)^{q-q''} \\ &\times C_{F_f}^{i_f}(J_a I_s, \mu_f) C_{F_a}^{i_a}(J_a I_s, \mu_a) \\ &\times C_{F_b}^{i_b}(J_b I_s, \mu_b) C_{F_{b''}}^{i_{b''}}(J_b I_s, \mu_{b''}) (2J_a + 1) \\ &\times \sqrt{(2F_a + 1)(2F_f + 1)(2F_b + 1)(2F_{b''} + 1)} \\ &\times \begin{pmatrix} F_b & F_f & 1 \\ -\mu_b & \mu_f & -q \end{pmatrix} \begin{pmatrix} F_{b''} & F_a & 1 \\ -\mu_{b''} & \mu_a & -q'' \end{pmatrix} \\ &\times \begin{Bmatrix} J_a & J_b & 1 \\ F_b & F_f & I_s \end{Bmatrix} \begin{Bmatrix} J_a & J_b & 1 \\ F_{b''} & F_a & I_s \end{Bmatrix} \\ &\times \varepsilon_q^{\alpha*} \varepsilon_{q''}^{\beta} \Phi_{\gamma}(\nu_{i_b \mu_b i_f \mu_f} - \xi) . \end{aligned} \quad (12)$$

Here,  $\varepsilon$  are the spherical vector components of the polarization unit vectors with  $\alpha$  and  $\beta$  referring

to the scattered and incident rays, respectively.  $\Phi_{\gamma}(\nu_{i_b \mu_b i_f \mu_f} - \xi)$  is the frequency-normalized profile function given by

$$\Phi_{\gamma}(\nu_{i_b \mu_b i_f \mu_f} - \xi) = \frac{1/\pi i}{\nu_{i_b \mu_b i_f \mu_f} - \xi - i\gamma/4\pi} , \quad (13)$$

where we have used an abbreviation

$$\begin{aligned} \nu_{i_b \mu_b i_f \mu_f} &= \nu_{J_b I_s i_b \mu_b, J_a I_s i_f \mu_f} \\ &= \nu_{J_b J_a} + \frac{E_{i_b}(J_b I_s, \mu_b) - E_{i_f}(J_a I_s, \mu_f)}{h} , \end{aligned} \quad (14)$$

with  $h$  being the Planck constant. The energy eigenvalues  $E$  and the expansion coefficients  $C$  are obtained by diagonalizing the total Hamiltonian given in Equation (3) (see Landi Degl’Innocenti 1978).

We then take the bilinear product of the matrix elements  $w_{\alpha\beta}$ , which involves performing coherent summation over the intermediate substates  $b$ . Furthermore, we perform incoherent summations over initial ( $a$ ) and final ( $f$ ) substates to form the coherency matrix and transform it to the laboratory frame, following the steps described in Section 2.2 of Sampoorna et al. (2007a). With the help of Equation (3.84) of Stenflo (1994) and the steps given in Appendix C of Sampoorna et al. (2007b), we express the coherency matrix in terms of irreducible spherical tensors  $\mathcal{T}_Q^K(i, \mathbf{n})$  introduced to polarimetry by Landi Degl’Innocenti (1984). Here,  $i = 0, 1, 2, 3$  refer to the Stokes parameters,  $K = 0, 1, 2$ , with  $Q$  taking  $(2K + 1)$  values, and  $\mathbf{n}$  is the direction of the scattered ray. The coherency matrix is then transformed to Stokes vector basis following the steps in Appendix C of Sampoorna et al. (2007b) to obtain

$$S_i = \sum_{j=0}^3 \mathbf{R}_{ij}^{\text{II}}(x, \mathbf{n}, x', \mathbf{n}'; \mathbf{B}) S'_j , \quad (15)$$

where  $S_i$  and  $S'_j$  are the Stokes vectors for the scattered and incident rays, respectively,  $\mathbf{R}_{ij}^{\text{II}}$  is the normalized RM for type II scattering in the laboratory frame and is given by

$$\begin{aligned} \mathbf{R}_{ij}^{\text{II}}(x, \mathbf{n}, x', \mathbf{n}'; \mathbf{B}) &= \frac{3(2J_b + 1)}{(2I_s + 1)} \\ &\times \sum_{K K' Q} \sum_{i_a \mu_a i_f \mu_f i_b \mu_b i_{b'} \mu_{b'}} \end{aligned}$$

$$\begin{aligned}
& \times \sum_{F_a F_{a'} F_f F_{f'} F_b F_{b'} F_{b''} F_{b'''} q q' q'' q'''} (-1)^{q-q'''+Q} \\
& \times \sqrt{(2K+1)(2K'+1)} \cos \beta_{i_b' \mu_{b'} i_b \mu_b} e^{i\beta_{i_b' \mu_{b'} i_b \mu_b}} \\
& \times [(h_{i_b \mu_b, i_b' \mu_{b'}}^{\text{II}})_{i_a \mu_a i_f \mu_f} + i(f_{i_b \mu_b, i_b' \mu_{b'}}^{\text{II}})_{i_a \mu_a i_f \mu_f}] \\
& \times C_{F_f}^{i_f}(J_a I_s, \mu_f) C_{F_a}^{i_a}(J_a I_s, \mu_a) C_{F_b}^{i_b}(J_b I_s, \mu_b) \\
& \times C_{F_{b''}}^{i_b}(J_b I_s, \mu_b) C_{F_{f'}}^{i_f}(J_a I_s, \mu_f) C_{F_{a'}}^{i_a}(J_a I_s, \mu_a) \\
& \times C_{F_{b'}}^{i_b'}(J_b I_s, \mu_{b'}) C_{F_{b'''}}^{i_b'}(J_b I_s, \mu_{b'}) \\
& \times \sqrt{(2F_a+1)(2F_f+1)(2F_{a'}+1)(2F_{f'}+1)} \\
& \times \sqrt{(2F_b+1)(2F_{b'}+1)(2F_{b''}+1)(2F_{b'''}+1)} \\
& \times \begin{pmatrix} F_b & F_f & 1 \\ -\mu_b & \mu_f & -q \end{pmatrix} \begin{pmatrix} F_{b'} & F_{f'} & 1 \\ -\mu_{b'} & \mu_{f'} & -q' \end{pmatrix} \\
& \times \begin{pmatrix} F_{b''} & F_a & 1 \\ -\mu_b & \mu_a & -q'' \end{pmatrix} \begin{pmatrix} F_{b'''} & F_{a'} & 1 \\ -\mu_{b'} & \mu_a & -q''' \end{pmatrix} \\
& \times \begin{pmatrix} 1 & 1 & K \\ q & -q' & -Q \end{pmatrix} \begin{pmatrix} 1 & 1 & K' \\ q''' & -q'' & Q \end{pmatrix} \\
& \times \begin{Bmatrix} J_a & J_b & 1 \\ F_b & F_f & I_s \end{Bmatrix} \begin{Bmatrix} J_a & J_b & 1 \\ F_{b'} & F_{f'} & I_s \end{Bmatrix} \\
& \times \begin{Bmatrix} J_a & J_b & 1 \\ F_{b''} & F_a & I_s \end{Bmatrix} \begin{Bmatrix} J_a & J_b & 1 \\ F_{b'''} & F_{a'} & I_s \end{Bmatrix} \\
& \times (-1)^Q \mathcal{T}_{-Q}^K(i, \mathbf{n}) \mathcal{T}_Q^{K'}(j, \mathbf{n}'). \quad (16)
\end{aligned}$$

Equation (16) represents the PRD matrix for hyperfine interaction in the PB regime. This equation, when written in the atomic rest frame, can be directly obtained from Equation (12) of Landi Degl'Innocenti et al. (1997) by introducing the spherical tensors and by assuming that the lower levels are unpolarized. The PRD matrix derived in this section satisfies the symmetry relations described in detail in Bommier (1997). In the above expression, the so-called Hanle angle  $\beta_{i_b' \mu_{b'} i_b \mu_b}$  is given by

$$\tan \beta_{i_b' \mu_{b'} i_b \mu_b} = \frac{\nu_{i_b' \mu_{b'} i_a \mu_a} - \nu_{i_b \mu_b i_a \mu_a}}{\gamma/2\pi}. \quad (17)$$

The auxiliary functions  $h^{\text{II}}$  and  $f^{\text{II}}$  appearing in Equation (16) have the form

$$\begin{aligned}
& (h_{i_b \mu_b, i_b' \mu_{b'}}^{\text{II}})_{i_a \mu_a i_f \mu_f} \\
& = \frac{1}{2} [R_{i_b \mu_b i_a \mu_a i_f \mu_f}^{\text{II,H}} + R_{i_b' \mu_{b'} i_a \mu_a i_f \mu_f}^{\text{II,H}}], \quad (18)
\end{aligned}$$

and

$$\begin{aligned}
& (f_{i_b \mu_b, i_b' \mu_{b'}}^{\text{II}})_{i_a \mu_a i_f \mu_f} \\
& = \frac{1}{2} [R_{i_b' \mu_{b'} i_a \mu_a i_f \mu_f}^{\text{II,F}} - R_{i_b \mu_b i_a \mu_a i_f \mu_f}^{\text{II,F}}], \quad (19)
\end{aligned}$$

where the magnetic redistribution functions of type II are defined as

$$\begin{aligned}
& R_{i_b \mu_b i_a \mu_a i_f \mu_f}^{\text{II,H}}(x_{ba}, x'_{ba}, \Theta) = \frac{1}{\pi \sin \Theta} \\
& \times \exp \left\{ - \left[ \frac{x_{ba} - x'_{ba} + x_{i_a \mu_a i_f \mu_f}}{2 \sin(\Theta/2)} \right]^2 \right\} \\
& \times H \left( \frac{a}{\cos(\Theta/2)}, \frac{x_{ba} + x'_{ba} + x_{i_a \mu_a i_f \mu_f}}{2 \cos(\Theta/2)} \right), \quad (20)
\end{aligned}$$

and

$$\begin{aligned}
& R_{i_b \mu_b i_a \mu_a i_f \mu_f}^{\text{II,F}}(x_{ba}, x'_{ba}, \Theta) = \frac{1}{\pi \sin \Theta} \\
& \times \exp \left\{ - \left[ \frac{x_{ba} - x'_{ba} + x_{i_a \mu_a i_f \mu_f}}{2 \sin(\Theta/2)} \right]^2 \right\} \\
& \times 2F \left( \frac{a}{\cos(\Theta/2)}, \frac{x_{ba} + x'_{ba} + x_{i_a \mu_a i_f \mu_f}}{2 \cos(\Theta/2)} \right). \quad (21)
\end{aligned}$$

Here,  $\Theta$  is the scattering angle; the functions  $H$  and  $F$  are the Voigt and Faraday-Voigt functions (see Equation (18) of Smitha et al. 2011). The quantities appearing in the expressions for the type II redistribution functions have the following definitions:

$$\begin{aligned}
& x_{ba} = \frac{\nu_{i_b \mu_b i_a \mu_a} - \nu}{\Delta \nu_D}; \quad x'_{ba} = \frac{\nu_{i_b \mu_b i_a \mu_a} - \nu'}{\Delta \nu_D}, \\
& x_{i_a \mu_a i_f \mu_f} = \frac{\nu_{i_a \mu_a i_f \mu_f}}{\Delta \nu_D}; \quad a = \frac{\gamma}{4\pi \Delta \nu_D}, \quad (22)
\end{aligned}$$

where  $x_{ba}$  is the emission frequency,  $a$  is the damping parameter, and  $\Delta \nu_D$  is the Doppler width.

We remark that the PRD matrix in the PB regime presented in this section can also be obtained by an alternative approach (see Shapiro et al. 2007) that avoids the use of statistical tensors  $\mathcal{T}_Q^K$ .

### 3.2. Special Cases

The PB theory and the relevant RM derived in Section 3.1 gives exact PRD matrix for the problem at hand. However, it is possible, under limiting cases, to derive simple expressions for practical applications. One example of this is the so-called Zeeman regime. In this regime, the magnetic field is so weak that it produces a splitting which is much smaller than the energy differences between the  $F$  states. In such a case, the magnetic Hamiltonian can be diagonalized analytically using the perturbation theory.

In the Zeeman regime where the basis vector is  $|J I_s F \mu\rangle$  in which  $F$  is a good quantum number, the RM in Equation (16) takes the form

$$\begin{aligned}
\mathbf{R}_{ij}^{\text{II}}(x, \mathbf{n}, x', \mathbf{n}'; \mathbf{B}) &= \frac{3(2J_b + 1)}{2I_s + 1} \\
&\times \sum_{KK'Qqq'q''q'''} (-1)^{q-q'''+Q} \\
&\times \cos \beta_{F_b' \mu_{b'}, F_b \mu_b} e^{i\beta_{F_b' \mu_{b'}, F_b \mu_b}} \\
&\times \left[ (h_{F_b \mu_b, F_b' \mu_{b'}}^{\text{II}})_{F_a \mu_a F_f \mu_f} + i(f_{F_b \mu_b, F_b' \mu_{b'}}^{\text{II}})_{F_a \mu_a F_f \mu_f} \right] \\
&\times (2F_a + 1)(2F_f + 1)(2F_b + 1)(2F_{b'} + 1) \\
&\times \sqrt{(2K + 1)(2K' + 1)} \\
&\times \begin{Bmatrix} J_a & J_b & 1 \\ F_b & F_f & I_s \end{Bmatrix} \begin{Bmatrix} J_a & J_b & 1 \\ F_b & F_a & I_s \end{Bmatrix} \\
&\times \begin{Bmatrix} J_a & J_b & 1 \\ F_{b'} & F_f & I_s \end{Bmatrix} \begin{Bmatrix} J_a & J_b & 1 \\ F_{b'} & F_a & I_s \end{Bmatrix} \\
&\times \begin{pmatrix} F_b & F_a & 1 \\ -\mu_b & \mu_a & -q'' \end{pmatrix} \begin{pmatrix} F_b & F_f & 1 \\ -\mu_b & \mu_f & -q \end{pmatrix} \\
&\times \begin{pmatrix} F_{b'} & F_a & 1 \\ -\mu_{b'} & \mu_a & -q''' \end{pmatrix} \begin{pmatrix} F_{b'} & F_f & 1 \\ -\mu_{b'} & \mu_f & -q' \end{pmatrix} \\
&\times \begin{pmatrix} 1 & 1 & K \\ q & -q' & -Q \end{pmatrix} \begin{pmatrix} 1 & 1 & K' \\ q''' & -q'' & Q \end{pmatrix} \\
&\times (-1)^Q \mathcal{T}_{-Q}^K(i, \mathbf{n}) \mathcal{T}_Q^{K'}(j, \mathbf{n}') . \tag{23}
\end{aligned}$$

The Hanle angle  $\beta_{F_b' \mu_{b'}, F_b \mu_b}$  is given by

$$\tan \beta_{F_b' \mu_{b'}, F_b \mu_b} = \frac{\omega_{F_b' F_b} + (g_{F_b'} \mu_{b'} - g_{F_b} \mu_b) \omega_L}{\gamma} , \tag{24}$$

where  $\omega_L$  is the Larmour frequency associated with the applied magnetic field. The Landé factors  $g_F$  appearing in the above equation are defined as

$$g_F = g_J \frac{1}{2} \frac{F(F+1) + J(J+1) - I_s(I_s+1)}{F(F+1)} , \tag{25}$$

for  $F \neq 0$ . Here,  $g_J$  is the  $L - S$  coupling Landé factor given by

$$g_J = 1 + \frac{1}{2} \frac{J(J+1) - L(L+1) + S(S+1)}{J(J+1)} . \tag{26}$$

Equation (23) has a formal resemblance to the Equation (25) derived in Smitha et al. (2011) for the case of  $J$ -state interference. Indeed, the  $F$ -state interference RM in the Zeeman regime can be obtained from the corresponding  $J$ -state interference RM through the replacement of  $(J, L, S)$

by  $(F, J, I_s)$  in the latter RM. When the magnetic field is set to zero in Equation (23), it takes the same form as Equation (2) of Smitha et al. (2012).

#### 4. SINGLE-SCATTERING REDISTRIBUTION

To study the behavior of the  $F$ -state RM derived for arbitrary field strengths, we consider the atomic line with the following configuration, namely, the Na I D<sub>2</sub> line resulting from the transition between  $J_a = 1/2$  and  $J_b = 3/2$ . The wavelength in air corresponding to this transition is  $\lambda_0 = 5889.95095 \text{ \AA}$ . The nuclear spin  $I_s = 3/2$ . The  $J - I_s$  coupling results in the hyperfine structure states  $F_b = 0, 1, 2, 3$  for the upper state  $J_b$  and  $F_a = 1, 2$  for the lower state  $J_a$ . The energies of these  $F$  states are taken from Steck (2003). When the degeneracy of the magnetic substates of the  $F$  states is lifted by the magnetic field, 68 allowed transitions take place between them in the PB regime. The hyperfine structure constants have the values  $\mathcal{A}_{1/2} = 885.81 \text{ MHz}$ ,  $\mathcal{B}_{1/2} = 0$ ,  $\mathcal{A}_{3/2} = 18.534 \text{ MHz}$ , and  $\mathcal{B}_{3/2} = 2.724 \text{ MHz}$  (see Steck 2003). The Einstein  $A$  coefficient for the  $J_b = 3/2$  state is taken to be  $6.3 \times 10^7 \text{ s}^{-1}$ . The Doppler width  $\Delta\lambda_D = 25 \text{ m\AA}$  and the damping parameter  $a = 0.00227$  (a value obtained after using  $\gamma = 6.3 \times 10^7 \text{ s}^{-1}$  in Equation (22), where  $a$  is defined) for all the components. The system that we have considered obeys the spacing rule described in Section 2. We study the results of a single  $90^\circ$  scattering event in which the unpolarized incident beam is scattered by this atomic system in a direction perpendicular to the incident beam.

##### 4.1. Polarization Diagram

The scattering geometry used for the calculation of the polarization diagrams (plots of  $Q/I$  vs  $U/I$ ) in the present section is shown in Figure 1. This geometry is identical to the one considered in Figure 5.11 of LL04. To explore the effects of the magnetic field in the PB regime on the linear polarization, we present in Figure 2 polarization diagrams computed at different distances from the line center. To construct these diagrams, we first compute the elements of the RM for a given value of  $B$  and integrate the first column of the RM over incident wavelengths.

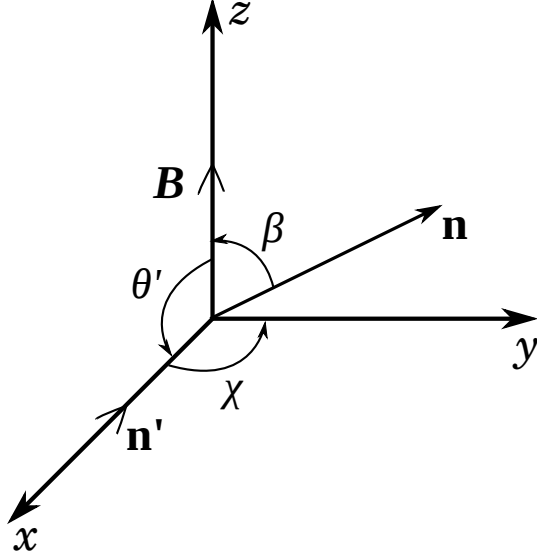


Fig. 1.— Geometry considered for polarization diagrams.  $\beta$  is the angle between the magnetic field vector and the scattered beam. The incident radiation is characterized by  $(\theta', \chi') = (90^\circ, 0^\circ)$  and the scattered radiation by  $(\theta, \chi) = (\beta, 90^\circ)$ . The magnetic field inclination  $\theta_B = 0^\circ$  and its azimuth  $\chi_B = 0^\circ$  (magnetic reference frame).

$F_b \backslash F_{b'}$		2	3	3	3
	$\mu_b \backslash \mu_{b'}$	-2	-3	-2	-1
1	0	<b>12.7</b>	31.3	...	...
1	+1	15	36	...	...
2	-1	...	<b>25.1</b>	...	...
2	0	...	16.3	<b>22</b>	52
2	+1	...	14	20	<b>44.5</b>
2	+2	...	13.3	18	37.8

Table 1: Magnetic field strengths (approximate values in G) for which the magnetic substates of the  $F$ -states cross. For instance, the crossing between  $\mu_b = 0$  of  $F_b = 1$  and  $\mu_{b'} = -2$  of  $F_{b'} = 2$  occurs at  $B \sim 12.7$  G. The numbers highlighted in boldface correspond to the field strength values for which level crossings occur when one considers the geometry given in Figure 1, i.e., the level crossings corresponding to  $\Delta\mu = \pm 2$ .

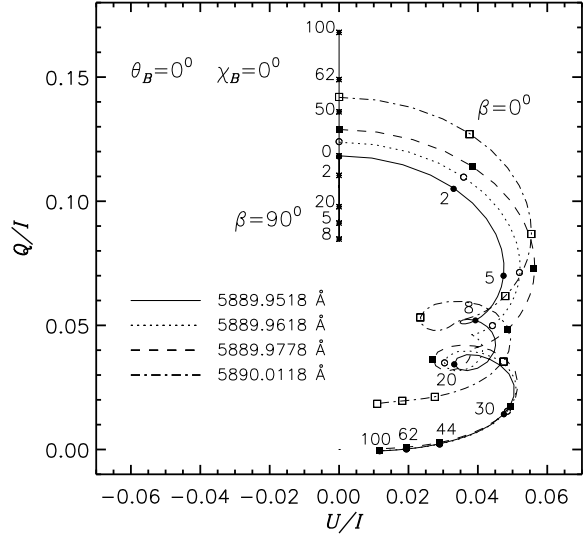


Fig. 2.— Hanle diagrams obtained for  $\beta = 0^\circ$  at different distances from the line center as indicated in the figure. The solid vertical line represents the  $\beta = 90^\circ$  case corresponding to the line center wavelength. The numbers along the solid curves represent the value of magnetic field strength  $B$  in G. The symbols on the other curves mark the same values of  $B$  as indicated for the solid curve for  $\beta = 0^\circ$ . The zero field point is the same for the two cases represented by solid lines.

The solid curve for  $\beta = 0^\circ$  (magnetic field parallel to the scattered beam) matches closely with the Hanle diagram shown in Figure 10.30 of LL04. As discussed in LL04, the loops seen in the polarization diagram arise due to the level crossings that occur in the PB regime. For the atomic system considered here, the level crossing diagram is identical to that in Figure 3.11 of LL04. The magnetic field strengths (in G) for which the level crossings occur are given in Table 1. For the geometry considered, level crossings take place only between magnetic substates with  $|\Delta\mu| = 2$ . The magnetic field values for which these crossings occur are highlighted in boldface in Table 1. The coherence between the overlapping substates increases around these values of field strengths. This leads to an increase in the scattering polarization toward its non-magnetic value, resulting in the formation of loops.

We see from the figure an overall increase in  $Q/I$  and  $U/I$  as we move away from the line center when  $\beta = 0^\circ$ . Furthermore, the upper loop (near 8 G) seen in the solid line case disappears for wavelengths away from the line center. On the other hand, the lower loop (near 20 G) becomes bigger in size. In the far wings of the line, the polarization diagram becomes a point corresponding to the Rayleigh case at  $Q/I = 0.428$  and  $U/I = 0$ .

In Figure 2, we also present the case of  $\beta = 90^\circ$  (magnetic field perpendicular to the scattering plane). In this case, the Hanle effect in a two-level atom with HFS shows an interesting phenomenon (see the vertical solid line) called anti-level crossing, which has been extensively studied and characterized in the case of CRD (Bommier 1980, LL04, p. 604). We see that the  $Q/I$  initially decreases from 0.118 at  $B = 0$  to nearly 0.0847 for  $B = 8$  G. With further increase in  $B$ , the  $Q/I$  starts increasing and exceeds its value at  $B = 0$ . Thus, we see that

$$\left(\frac{Q}{I}\right)_{B=0}^{I_s \neq 0} < \left(\frac{Q}{I}\right)_{B \rightarrow \infty}^{I_s \neq 0}. \quad (27)$$

This occurs due to the basis transformation of the energy eigenstates in the complete PB regime. The basis transformation takes place when the field strength increases from incomplete PB regime to the complete PB regime. In the incomplete PB regime, the energy eigenstates are given by  $|JI_s i\mu\rangle$ , whereas in the complete PB regime they

are given by  $|J\mu_J I_s \mu_{I_s}\rangle$ . Anti-level crossing is also known as avoided crossing, in which, due to the strong coupling of the  $J$  and  $I_s$  to the magnetic field, the magnetic substates instead of crossing, repel each other. Due to the geometry of the problem,  $U/I$  is zero.

## 4.2. Stokes Profiles in the PB Regime

In this section, we present the Stokes profiles computed with PRD. Sections 4.2.1, 4.2.2, and 4.2.3 show the Stokes profiles obtained for various magnetic field configurations. The magnetic field orientations are discussed in the text and strengths are indicated in the figures. The incident radiation is characterized by  $(\cos \theta', \chi') = (0, 0^\circ)$  and the scattered ray by  $(\cos \theta, \chi) = (0, 90^\circ)$ . For the computation of the Stokes profiles, we use a wavelength grid having 376 finely spaced points covering a bandwidth of 2 Å. The separation between the  $F$  states in the absence of a magnetic field is of the order of mÅ. In the presence of a magnetic field, the magnetic components are shifted away from the line center and the wavelength grid that we have considered is good enough and covers all the components shifted by the magnetic field.

### 4.2.1. Vertical Magnetic Field Perpendicular to the Line of Sight

In Figure 3, the left panels show the Stokes profiles obtained for different strengths of a vertical magnetic field ( $\theta_B = 0^\circ$  and  $\chi_B = 0^\circ$ ). We see that the intensity increases slightly with increasing field strength.  $Q/I$  profiles show a decrease in amplitude up to 8 G (see short dashed line). For stronger fields (greater than 8 G), the  $Q/I$  amplitude increases (see also Figure 2). This is the signature of anti-level crossing effect which occurs because of the repulsion between the magnetic substates. As discussed earlier, as a result of this effect, the  $Q/I$  line core value, when considered as a function of field strength, initially decreases and then increases beyond its non-magnetic value. Transverse Zeeman effect signatures show up prominently for fields stronger than 100 G. Because of the geometry considered,  $U/I$  is zero.



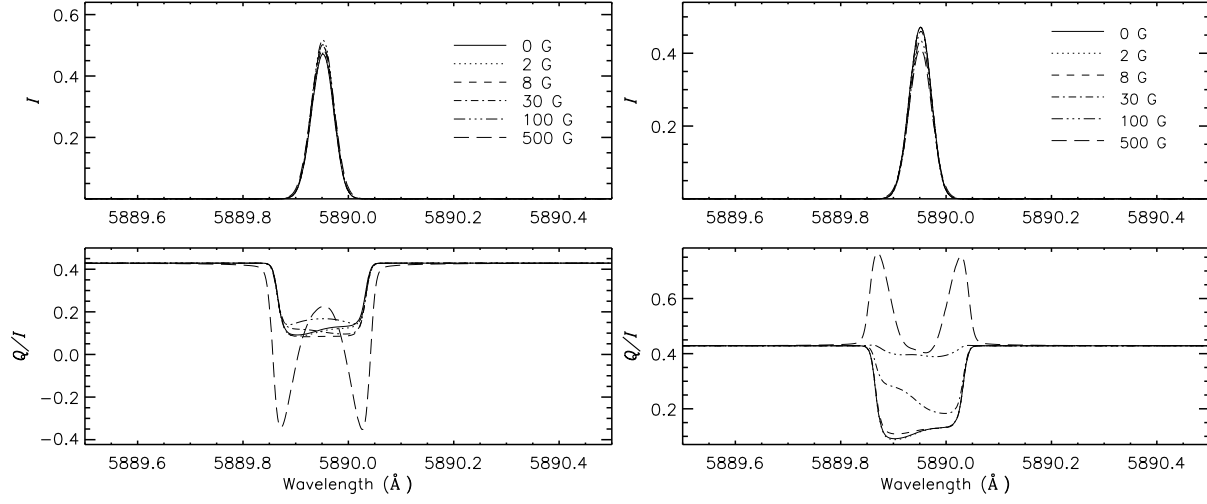


Fig. 3.— Stokes profiles computed for the case of a vertical magnetic field (left panels) and for the case of a horizontal magnetic field perpendicular to the line of sight (right panels).

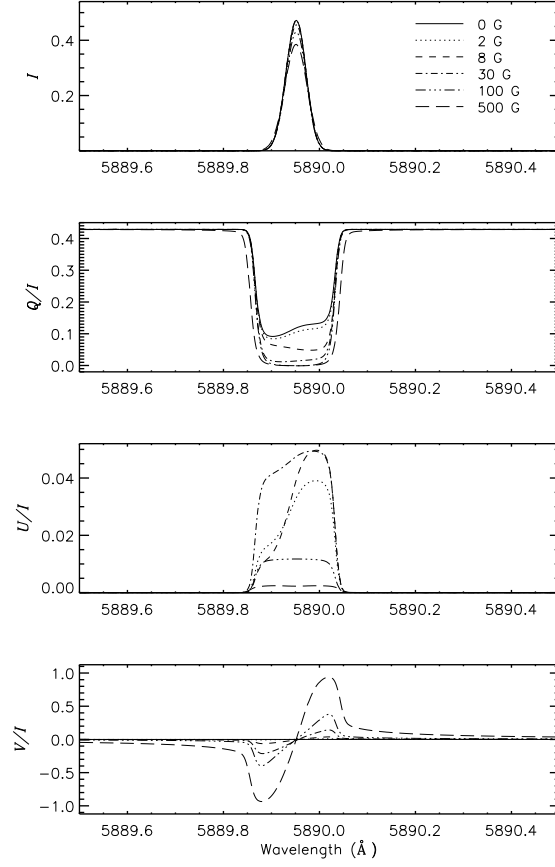


Fig. 4.— Stokes profiles computed for the case of a horizontal magnetic field parallel to the line of sight.

#### 4.2.2. Horizontal Magnetic Field Perpendicular to the Line of Sight

The case of a horizontal field perpendicular to the line of sight ( $\theta_B = 90^\circ$  and  $\chi_B = 0^\circ$ ) is shown in the right panels of Figure 3. We see that the intensity decreases monotonically with field strength.  $Q/I$  profiles show an increase in amplitude from their Rayleigh scattered values with an increase in the field strength. For fields of the order of 100 G and larger, we see three lobed profiles in  $Q/I$  due to transverse Zeeman effect. Once again,  $U/I$  is zero due to the geometry.

#### 4.2.3. Horizontal Magnetic Field Parallel to the Line of Sight

For this geometry of the magnetic field ( $\theta_B = 90^\circ$  and  $\chi_B = 90^\circ$ ), the intensity profiles behave in the same way as in the case of a horizontal field perpendicular to the line of sight (see Figure 4). The depolarization in the line core due to the Hanle effect is clearly visible in the  $Q/I$  panel. The  $U/I$  signal is now generated because of Hanle rotation. There is an increase in  $U/I$  amplitude for weaker fields and then a decrease for stronger fields, which is a typical signature of the Hanle effect. We notice that the  $V/I$  profiles are asymmetric in the incomplete PB regime (for fields up to 200 G) while it is perfectly anti-symmetric in the complete PB regime (for fields greater than 200 G). This is because incomplete PBE shifts the magnetic components asymmetrically about the line center and causes differential strengths for these components. Because of this asymmetry, the net circular polarization (NCP), defined as  $\int V d\lambda$  (where the integration is done over the full line profile), is non-zero (the NCP would be zero if the splitting produced by the magnetic field is symmetric). For the atomic line under consideration, NCP remains non-zero up to 200 G.

## 5. CONCLUSIONS

LL04 incorporated the PBE on the hyperfine structure states in the polarization studies under the assumption of CRD. They assume that the incident radiation is independent of frequency in an interval larger than the frequency shifts and inverse lifetimes of the hyperfine structure substates involved in the transitions (flat-spectrum approximation). In the present paper, we have consid-

ered the same problem, but for the case of PRD. This allows us to handle the frequency dependence of the incident radiation field (relaxation of flat-spectrum approximation). In this way, the Stokes profile shapes can be properly calculated by including the effects of PRD. We have derived the PRD matrix for  $F$ -state interference process, in the collisionless regime, in the presence of magnetic fields of arbitrary strengths.

Through the polarization diagrams computed at different scattered wavelengths, we have shown the dependence on wavelength of the loops which are characteristics of level crossings that occur in the PB regime. With the help of the Stokes profiles computed for the case of a vertical magnetic field, we have also demonstrated the anti-level crossing effect, which was discussed for the case of CRD by Bommier (1980) and LL04. Based on the formulation described in the present paper, it is possible to use the diagnostic potential of PBE with PRD, in a complementary way with the Zeeman effect, to determine the strengths and geometry of the magnetic fields in the solar atmosphere.

We thank Ms. H. N. Smitha for her help and useful discussions. We also acknowledge the use of HYDRA cluster at the Indian Institute of Astrophysics for computing. We are grateful to the referee for very useful comments and suggestions which helped to improve the paper substantially.

## REFERENCES

- Asensio Ramos, A. 2006, in ASP Conf. Ser. 358, Solar Polarization 4, ed. R. Casini & B. W. Lites (San Francisco, CA: ASP), 301
- Belluzzi, L. 2009, A&A, 508, 933
- Belluzzi, L., Trujillo Bueno, J., & Landi Degl’Innocenti, E. 2007, ApJ, 666, 588
- Berdyugina, S. V., Braun, P. A., Fluri, D. M., & Solanki, S. K. 2005, A&A, 444, 947
- Berdyugina, S. V., Fluri, D. M., Ramelli, R., et al. 2006a, ApJL, 649, L49
- Berdyugina, S. V., Fluri, D. M., & Solanki, S. K. 2006b, in ASP Conf. Ser. 358, Solar Polarization 4, ed. R. Casini & B. W. Lites (San Francisco, CA: ASP), 329
- Bommier, V. 1980, A&A, 87, 109

- Bommier, V. 1997, *A&A*, 328, 726
- Casini, R., & Manso Sainz, R. 2005, *ApJ*, 624, 1025
- Corney, A. 1977, *Atomic and Laser Spectroscopy* (Oxford: Oxford Univ. Press)
- Khalack, V., & Landstreet, J. D. 2012, *MNRAS*, 427, 569
- Landi Degl’Innocenti, E. 1975, *A&A*, 45, 269
- Landi Degl’Innocenti, E. 1978, *A&AS*, 33, 157
- Landi Degl’Innocenti, E. 1984, *SoPh*, 91, 1
- Landi Degl’Innocenti, E., Landi Degl’Innocenti, M., & Landolfi, M. 1997, in *Proc. Forum THEMIS, Science with THEMIS*, ed. N. Mein & S. Sahal Br  chot (Paris: Obs. Paris-Meudon), 59
- Landi Degl’Innocenti, E., & Landolfi, M. 2004, *Polarization in Spectral Lines* (Dordrecht: Kluwer) (LL04)
- Lopez Ariste, A., Tomczyk, S., & Casini, R. 2002, *ApJ*, 580, 519
- Sampoorna, M., Nagendra, K. N., & Stenflo, J. O. 2007a, *ApJ*, 663, 625
- Sampoorna, M., Nagendra, K. N., & Stenflo, J. O. 2007b, *ApJ*, 670, 1485
- Sasso, C., Lagg, A., & Solanki, S. K. 2006, *A&A*, 456, 367
- Shapiro, A. I., Fluri, D. M., Berdyugina, S. V., & Stenflo, J. O. 2006, in *ASP Conf. Ser. 358, Solar Polarization 4*, ed. R. Casini & B. W. Lites (San Francisco, CA: ASP), 311
- Shapiro, A. I., Fluri, D. M., Berdyugina, S. V., & Stenflo, J. O. 2007, *A&A*, 461, 339
- Smitha, H. N., Nagendra, K. N., Stenflo, J. O., & Sampoorna, M. 2013, *ApJ*, 768, 163
- Smitha, H. N., Sampoorna, M., Nagendra, K. N., & Stenflo, J. O. 2011, *ApJ*, 733, 4
- Smitha, H. N., Sowmya, K., Nagendra, K. N., Sampoorna, M., & Stenflo, J. O. 2012, *ApJ*, 758, 112
- Steck, D. A. 2003, *Sodium D Line Data* (Notes available at <http://steck.us/alkalidata/>)
- Stenflo, J. O. 1994, *Solar Magnetic Fields: Polarized Radiation Diagnostics* (Dordrecht: Kluwer)
- Stenflo, J. O. 1997, *A&A*, 324, 344
- Stenflo, J. O. 1998, *A&A*, 338, 301
- Stift, M. J., & Leone, F. 2008, *CoSka*, 38, 185
- Stift, M. J., Leone, F., & Landi Degl’Innocenti, E. 2008, *MNRAS*, 385, 1813
- Woodgate, G. K. 1992, *Elementary Atomic Structure* (Oxford: Oxford Univ. Press)